NICOLAUS COPERNICUS UNIVERSITY IN TORUŃ

Bulletin of Geography. Physical Geography Series, No. 30 (2026): 73–91
http://doi.org/10.12775/bgeo-2026-0005

Application of GIS-based bivariate statistic for prediction of landslide susceptibility mapping in Lindu District, Indonesia

Septianto Aldiansyah[1,2*][a], **Ilyas Madani**[2][b]

[1]Universitas Indonesia, Faculty of Mathematics and Natural Sciences, Department of Geography, Depok, Indonesia

[2]Universitas Halu Oleo, Faculty of Teacher Training and Education, Geography Education, Kendari, Indonesia

[3]Universitas Negeri Malang, Faculty of Social Science, Department of Geography, Malang, Indonesia

*E-mail: septiantoaldiansyah863@gmail.com

[a] https://orcid.org/0000-0002-5432-8322, [b] https://orcid.org/0000-0001-8908-3604

Abstract. This study utilized Geographic Information Systems (GIS) and bivariate statistical models to delineate landslide susceptibility in Lindu District, Indonesia. The results of Google Earth image interpretation and expert validation identified around 391 landslide locations and randomly classified into training (70%) and validation (30%) datasets. Fifteen landslide conditioning factors: elevation, slope, aspect, curvature, plan curvature, profile curvature, stream power index, topographic wetness index, road, river, fault, land use, normalized difference vegetation index, lithology and precipitation are combined with landslide training to obtain each factor weight and factor class from the Weight of Evidence (WoE) and Informative Value (IV) models. Both models were then validated using the area under curve (AUC). The AUC model accuracy results show that the success rates of the WoE and IV models are 81.93% and 80.36%, and the prediction rates are 80.83% and 77.35%, respectively. This study aids local governments in landslide risk mitigation planning.

Key words:
Susceptibility assessment, Mass movements, Bivariate models, Weight of Evidence, Informative Value

Introduction

In mountainous areas of Indonesia, landslides cause the greatest environmental damage and greatest threat to human life compared to other geological disasters (Ngadisih et al. 2017). Landslides are generally interpreted as movements of rocks, sediments or debris on slopes (Turner and Schuster 1996). The triggers for landslides are often attributed to natural disasters and human intervention, including earthquakes, road construction, deforestation or mineral exploitation (Hussain et al. 2019). According to global landslide statistics, several regions in Asia, including Indonesia, are considered to have been affected by quite destructive landslides in the last decade (Gómez et al. 2023). Indonesian Disaster Information Data (DIBI) (DIBI 2024) documents that 124 people died, 78 people were injured and 8,466 houses were severely damaged in 2024 due to landslides in Indonesia. Likewise, 12 landslide incidents occurred from 2018–2023 in Central Sulawesi, causing 16 people to die and damaging 22 houses. Providing an accurate and efficient landslide susceptibility map is considered to contribute significantly to mitigation and ensuring public safety, considering the significant high threat posed to the sustainability of human life and natural property. Indonesia has published numerous studies related to landslide susceptibility modeling in recent decades

(Subiyantoro et al. 2022). Among the various geodynamic phenomena, mass movements are identified as the most common processes affecting the region (Hadmoko et al. 2024).

The study area is reported to often undergo significant landslides due to development and resource management that ignores soil conservation. Therefore, we consider it necessary to conduct a landslide susceptibility analysis and compare the accuracy of various models in the Lindu District. The compiled landslide inventory indicates that more than 100 new and reactivated landslide events were detected in the Nokilalaki mountains prior to 2023 (Bagenda et al. 2020). Landslide susceptibility studies can provide spatial distribution of locations affected by landslides by involving several conditioning criteria (Brabb 1984). Conditioning factors such as topography, slope gradient, failure mechanism, extreme rainfall, land cover, geological formation, rock strength, and so on are considered responsible for the event. Models that are widely explored and adopted in landslide mapping include: inventory-based methods (Van Den Eeckhaut et al. 2005); bivariate statistical approaches, such as frequency ratio (FR) and statistical index; and multivariate models, including logistic regression (LR), cluster analysis and artificial neural networks (ANN) (Ayalew and Yamagishi 2005; Yilmaz 2009; Wang et al. 2016; Du et al. 2017; Tang et al. 2020; Zhang et al. 2020; Mehrabi and Moayedi 2021; Huang and Chen 2024). These models are considered to have provided fairly accurate predictions regarding landslides, and among them, bivariate statistical models, such as Weight of Evidence (WoE) and Informative Value (IV), are the more popular and have been studied extensively. WoE and IV methods can assess the individual contribution of factors quantitatively and in an interpretable manner by providing explicit logarithmic weights that allow researchers and policymakers to understand the influence of conditioning factors (Regmi et al. 2014; Bhandari et al. 2024). In contrast, ANN is often criticized for its implicit black-box nature (Yilmaz 2009; Martens et al. 2011). This situation makes policy applications or community-based management more difficult because it ignores transparency and interpretability (Lee and Pradhan 2007; Wang et al. 2016). The two models are often compared to determine which approach is the most accurate. In general, in more in-depth mapping, statistical methods such as WoE or generalized additive models, as well as various approaches to multi-criterion decision analysis (MCDA), regression analysis, and fuzzy sets can also be applied and compared (Ngadisih et al. 2017). Among these methods, WoE and IV are considered to have lower errors, in addition to the advantages of simpler implementation and greater ease of access.

Although both methods are bivariate and capable of handling categorical and discretized continuous variables, they differ in key aspects. Weight of Evidence is based on Bayesian probability and accounts for both the presence and absence of landslides (Ayalew et al. 2004), producing positive or negative weights that indicate whether a class increases or decreases landslide likelihood. Informative Value only considers landslide occurrence and does not explicitly include absence data, which may lead to less balanced outcomes (Yilmaz 2009; Umar et al. 2014). Furthermore, WoE assumes conditional independence among input variables, an assumption that requires correlation testing and potential exclusion of redundant factors, whereas IV does not impose such a condition, making it simpler but potentially less statistically robust in multicollinear settings (Yang et al. 2015).

Given these considerations, a comparative analysis between WoE and IV is required to understand which method performs more effectively under specific conditions and datasets. This study aims to examine landslide susceptibility prediction from two bivariate techniques, namely WoE and IV, in Lindu Regency, Indonesia. The information obtained from this study is expected to contribute to future land management and spatial planning in Lindu Regency. The development of landslide susceptibility maps is considered to support the identification of landslide-prone areas and determination of priority mitigation steps to reduce the impact of landslide disaster risks.

Study area

Lindu District is located in the north-east of the Nokilalaki mountains and covers 613.13 km^2. Based on the UTM Zone 51S coordinates, the area is located between 119°38'45"–120°21'24"E and 0°52'16"–2°03'21"S (Fig. 1). This area is in the altitude range of 763–2,373 m a.s.l., with Lake Lindu

 Citation: Bulletin of Geography. Physical Geography Series 2026, 30, http://doi.org/10.12775/bgeo-2026-0005

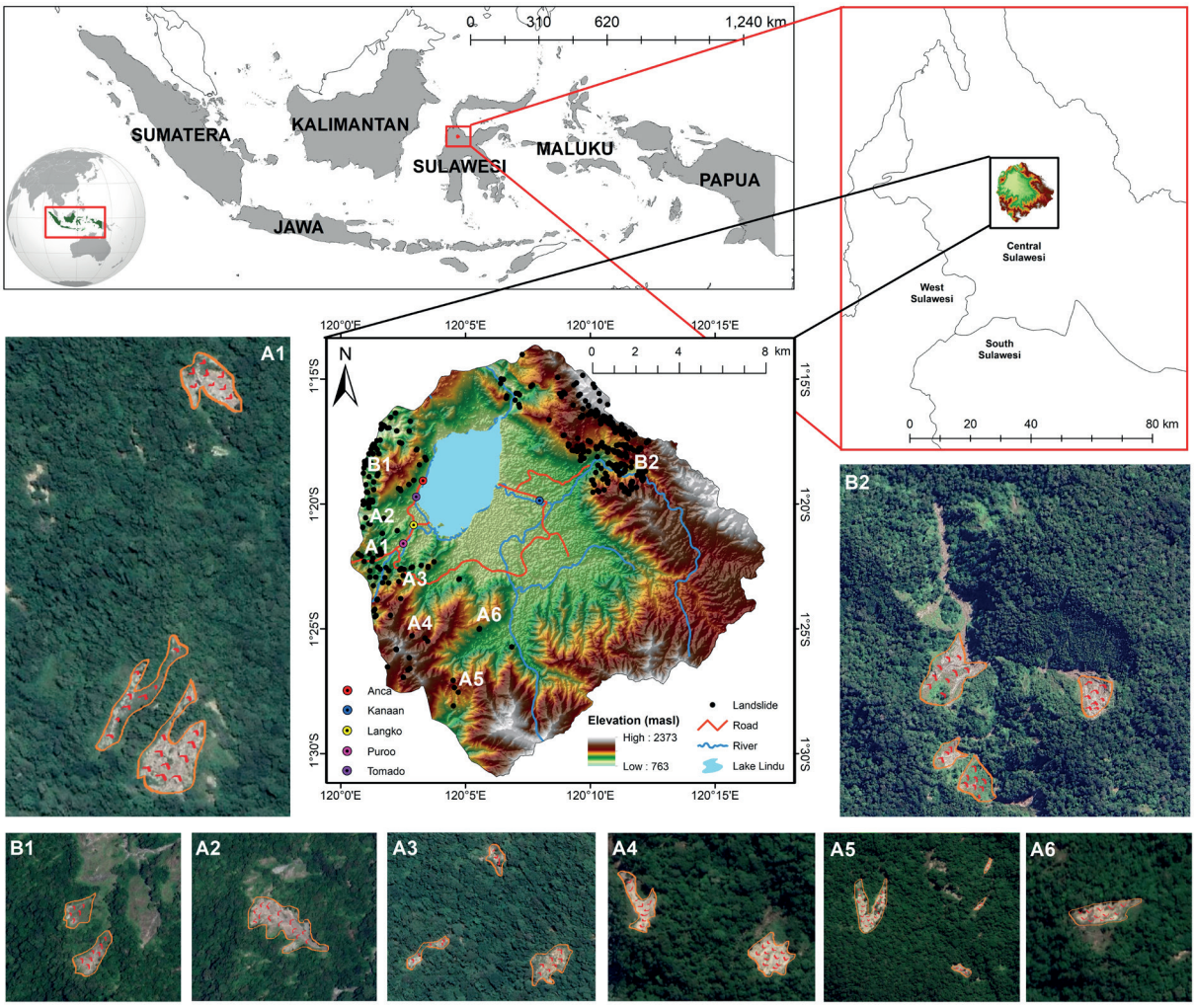

Fig. 1. Study area map showing landslide locations in Lindu, Central Sulawesi. Landslides are classified as seismically-triggered (A1–A6) and rainfall-triggered (B1–B2). Insets show detailed imagery of selected landslides

as the main feature. This main feature was formed due to geological activity during the Pliocene. The geological structure in the study area, such as the Palu-Koro fault, is related to non-volcanic geothermal potential and earthquakes (Jalin et al. 2021; Yusran et al. 2023). The research location mostly has a slope of 0–2°, which can inhibit the rate of rainwater runoff. However, extreme rainfall can still increase the possibility of landslides and floods. The average rainfall and temperature recorded were 164 mm and 21°C, respectively. Most of the area is covered by primary forest. The population in this area is 6,089 people, with a population density of 11.03 people/km² (BPS 2024). The activity centers are spread across five villages: Anca, Puroo, Langko, Tomado, and Kanaan, with Tomado as the sub-district government center.

Materials and methods

Data sources and methodology

This study utilizes two data sources. Primary data are obtained independently through surveys and field observations. Secondary data comprise data from institutions, articles, the internet and government documents. This study uses primary data from SRTM

30-m DEM data, Landsat-9 OLI II/TIRS II, and Google Earth imagery. Land use and NDVI data were extracted from Landsat 9 OLI-II/TIRS-II satellite imagery. SRTM DEM data were used to create elevation data layers. The elevation data were then derived into Slope, Curvature, Profile Curvature, Plan Curvature, Aspect, TWI and SPI data. Precipitation data were obtained from WorldClim 30 m. The lithology layer was obtained from the Ministry of Energy and Mineral Resources of Central Sulawesi. Proximity data were obtained from the Indonesian Geospatial Information Agency. All data layers were created and combined in the ArcGIS 10.4.1 application. All landslide susceptibility factors used are presented in Table 1, while the workflow of this study is illustrated in Figure 2.

Landslide inventory map

Landslide inventory maps were developed primarily through visual interpretation of satellite imagery (including Google Earth), supported by literature searches, technical reports, government data and expert interviews (Sivakami and Rajkumar 2020; Wubalem 2020). Direct, photographic documentation was not performed in the field, due to limited accessibility and safety considerations. However, expert-based validation and GPS-referenced information were used to support the spatial accuracy of landslide locations. This study used 391 landslide areas from data sources integrated with GPS in 2013–24, with

Table 1. The conditioning factors

Type of Conditioning factor	Format/Resolution/ Scale	Source
Elevation, slope, aspect, curvature, plan curvature, profile curvature, SPI and TWI	Raster (30 m)	SRTM DEM imagery
Road, River and Fault	Vector (1:50.000)	Geospatial Information Agency Indonesia
Land use and NDVI	Raster (30 m)	Landsat 9 OLI-II/TIRS-II in the USGS (2024)
Lithology	Vector (1:100.000)	Ministry of Energy and Mineral Resources of the Republic of Indonesia
Precipitation	Raster (30 m)	WorldClim ver 2.1 climate data for 1970–2000
Landslide area	Vector	Digitized from Google Earth imagery and expert-based validation

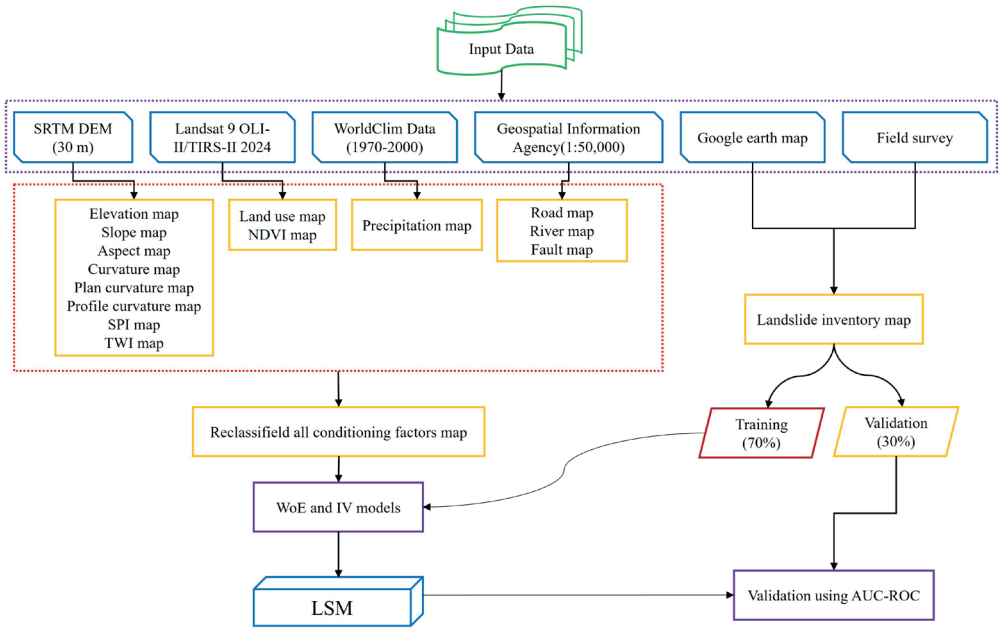

Fig. 2. Overall Methodology Workflow

Citation: Bulletin of Geography. Physical Geography Series 2026, 30, http://doi.org/10.12775/bgeo-2026-0005

a total area of 0.53 km^2. This landslide area is equivalent to the area of settlements, agricultural land and important transportation routes in Lindu district. The landslide types identified in this study follow the classification system of Hungr et al. (2014). Based on satellite interpretation and expert-based validation, five major types of landslides were recognized: rock falls, rock slides, debris flows, earth slides and soil flows. These classifications were selected to reflect the main triggering mechanisms observed in the study area. Based on expert validation, landslides in Lindu district were triggered by seismic activity (Fig. 1, A1–16) and heavy rainfall (Fig. 1, B1–B2). Specifically, rock-related failures such as rock falls and rock slides were predominantly triggered by seismic activity, whereas debris and soil flows were commonly associated with intense rainfall and the presence of riverbanks and saturated slopes.

Landslide conditioning factors

Identifying conditioning factors for landslides is complex, with no established guidelines for selecting factors (Ayalew and Yamagishi 2005). This study used 15 conditioning factors based on literature, effectiveness, data availability, and relevance to landslide events (Es-smairi et al. 2023; Aldiansyah and Wardani 2024a). These factors include elevation, slope, aspect, curvature, plan curvature, profile curvature, SPI, TWI, road, river, fault, land use, NDVI, lithology, and precipitation. Each factor was transformed into a raster format with uniform dimensions and categorized using the Jenks natural break method (Addis 2024) in ArcGIS (Fig. 3).

In landslide susceptibility studies, elevation influences human activities, vegetation, soil moisture, and climate (He et al. 2012; Shu et al. 2021). Slope gradient is a major cause of landslides (Wang et al. 2016; Du et al. 2017), with steeper slopes increasing landslide likelihood (Xu et al. 2012; Pham et al. 2017; Panchal and Shrivastava 2021). Curvature affects surface runoff and groundwater infiltration, influencing erosion and groundwater conditions (Oh et al. 2017; Aldiansyah and Wardani 2024a). Curvature is categorized as concave (–), convex (+) or flat (0), with more negative values indicating greater landslide potential (Lee and Choi 2004). Profile curvature refers to the vertical plane parallel to the slope (Ding et al. 2017), while plan curvature contributes to soil erosion or sliding in concave areas under excessive water pressure (Ding et al. 2017). Aspect, related to slope direction, affects erosion, evaporation, weathering, land aridity, and sun exposure, all influencing slope movement (Du et al. 2017; Khan et al. 2019). TWI, a key factor in landslide mapping, affects soil moisture distribution and landslide occurrence, derived from SRTM DEM data using Equation (1):

$$\mathrm{TWI} = \mathrm{Ln}\left(\frac{A_s}{\tan\beta}\right) \quad (1)$$

where A_s is the specific catchment area (m^2/m) and β is slope angle in degrees (Aldiansyah and Wardani 2024a).

The Stream Power Index (SPI) is an essential factor used to assess the erosive strength of water flow and the sediment transported by across the land (Aldiansyah and Wardani 2024a). SPI is calculated using the following Equation (2):

$$\mathrm{SPI} = AS \times \tan\beta \quad (2)$$

where AS is the slope contributing area and β is the slope angle.

Precipitation is one of the triggering factors for landslides (Dahal et al. 2012; Aldiansyah et al. 2023). The rainfall map was obtained from WorldClim data and re-interpolated using the IDW method. In highland areas, roads are often associated with the cause of landslides (Ngadisih et al. 2017). Building roads close to the slope is thought to alter the area's natural conditions. The river network also contributes to influencing landslides, especially those close to the water surface. Landslide distribution is correlated with tectonic fractures that will reduce rock strength. Landslides usually occur along faults, and the number of landslides decreases sharply as the distance from the fault increases (Xu et al. 2012; Aldiansyah and Wardani 2024a). The NDVI conditioning factor was extracted from Landsat 9 OLI-II/TIRS-II imagery with a spatial resolution of 30 m using the following Equation (3):

$$\mathrm{NDVI} = \frac{\mathrm{IR} - \mathrm{R}}{\mathrm{IR} + \mathrm{R}} \quad (3)$$

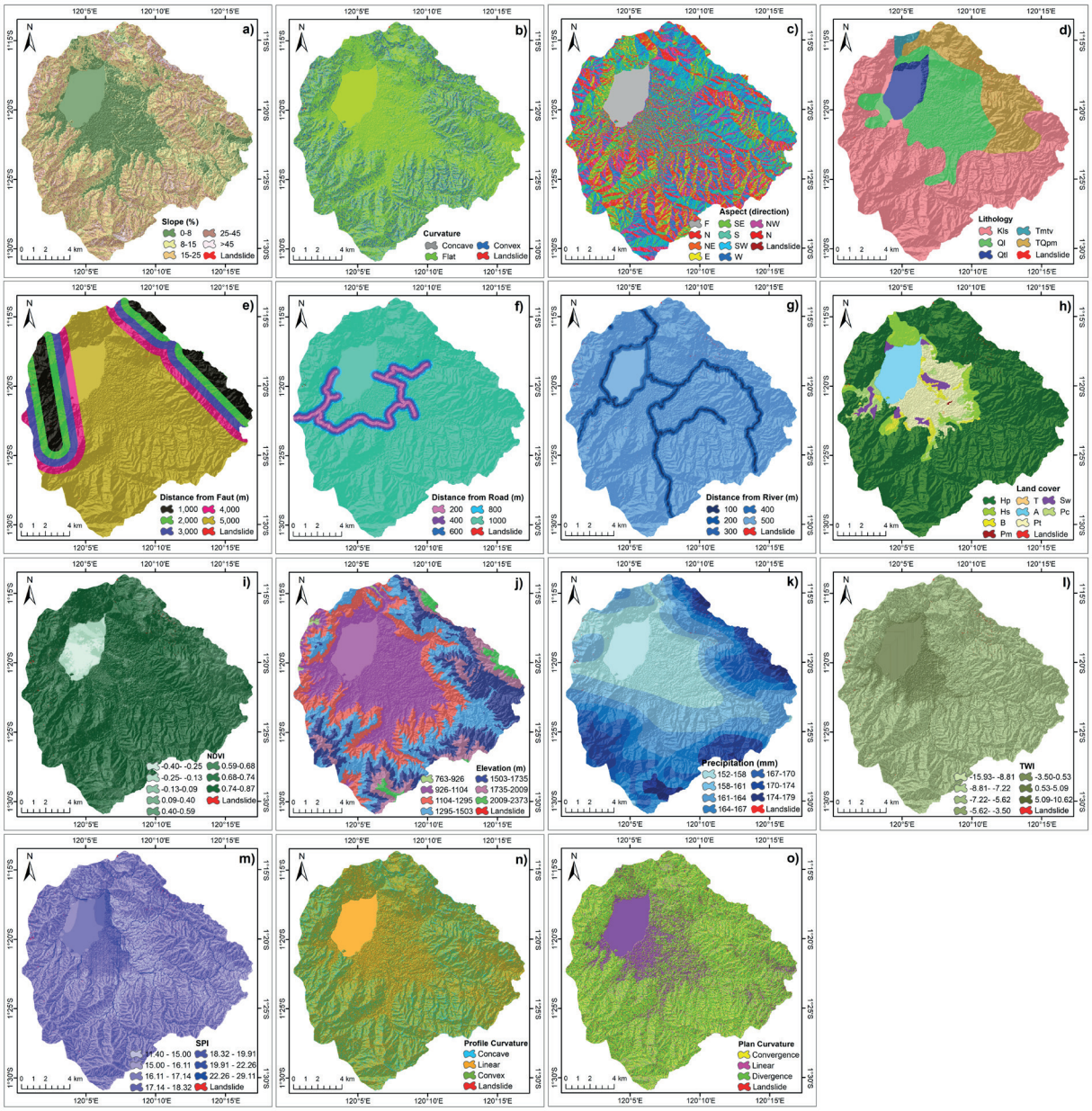

Fig. 3. Landslide conditioning factors: a) slope, b) curvature, c) aspect, d) lithology, e) distance from fault, f) distance from road, g) distance from river, h) land cover, i) NDVI, j) elevation, k) precipitation, l) TWI, m) SPI, n) profile curvature, o) plan curvature

where IR is the infrared and R is the red bands of the electromagnetic spectrum.

NDVI ranges from –1 to 1, with negative values typically being associated with clouds, water and snow. Meanwhile, values approaching zero indicate rocks and bare soil, whereas positive values indicate land covered by vegetation. Land use maps were obtained from supervised classification techniques on Landsat 9 OLI-II/TIRS-II images and categorized into nine classes. The large study area is mostly covered by primary forest. Lithology is categorized into five classes, and the dominant type is from the Latimojong Formation (Kls). The Latimojong Formation consists of alternating slate, phyllite, malih sandstone and local intercalations with malih mudstone.

Citation: Bulletin of Geography. Physical Geography Series 2026, 30, http://doi.org/10.12775/bgeo-2026-0005

Landslide susceptibility modeling

Weight of Evidence Model

The Weight of Evidence (WoE) method is a bivariate statistical method that was initially used to detect mineral location with a Bayesian log-linear approach (Lee and Choi 2004). This model uses the effect of slope instability in identifying the possibility of landslides that refer to the contribution of evidence (Dahal et al. 2012). The weight of each factor class category is determined based on the presence or absence of landslides (L).

$$\mathrm{W}^{+} = \ln \frac{P\left\{\frac{B}{L}\right\}}{P\left\{\frac{B}{L'}\right\}} \tag{4}$$

$$\mathrm{W}_{i} = \ln \frac{P\left\{\frac{B'}{L}\right\}}{P\left\{\frac{B'}{L'}\right\}} \tag{5}$$

where ln represents the logarithm and P denotes probability; B indicates the presence of a potential landslide factor; B' represents the absence of a potential landslide factor; L and L' refer to the presence and absence of a landslide, respectively.

The presence and absence of conditioning variables are indicated as W^{+} and W^{-} and are arrived at by Equations (6) and (7), respectively. Similarly, W^{+} and W^{-} indicate, respectively, the positive and negative correlations between conditioning variables and landslides. Once the W^{+} and W^{-} values are obtained, the weight contrast (C) is determined by subtracting W^{-} from W^{+}. The weight contrast (C) indicates the relationship between landslides and conditioning factors. The presence and absence of landslides in each conditioning factor and its subclasses are obtained in pixel units. Equations (6) and (7) are modified to calculate the pixel count.

$$W^{+} = \ln \left\{ \frac{\frac{A1}{A1+A2}}{\frac{A3}{A3+A4}} \right\} \tag{6}$$

$$W^{-} = \ln \left\{ \frac{\frac{A2}{A1+A2}}{\frac{A4}{A3+A4}} \right\} \tag{7}$$

where $A1$ is the landslide pixels present on a given factor class; $A2$ is the landslide pixels absent in the given factor class; $A3$ is the pixels in the specified factor class that do not include any landslide pixels; $A4$ is the number of pixels in which neither landslide nor the given factors are present.

The weights obtained are then used to obtain contrast values for certain vulnerability variables, which are formulated in Equation (8) as follows:

$$C = W^{+} - W^{-} \tag{8}$$

The contrast value (C), calculated as the difference between positive and negative weights, quantifies the strength and direction of the correlation between each conditioning factor and the occurrence of landslides.

Informative Value Model

Model IV is one of the bivariate statistical approaches that assess landslide vulnerability based objectively on information theory. Model IV works by assessing the spatial connection between the conditioning factor classes and the likelihood of landslide occurrence. The higher IV value indicates a stronger correlation between the probability of a landslide and the class of each conditioning factor. IV values greater than 0 suggest a higher probability of landslides, and vice versa. The landslide vulnerability at each pixel is calculated by summing up the values of each factor class. The derivation and mathematical relationship of this model are as follows:

$$\text{Conditioning probability } (Pc) = \frac{Si}{S} \tag{9}$$

$$\text{Prior probability } (Pp) = \frac{Ni}{N} \tag{10}$$

$$\text{Information Value } (IV) = \frac{Ni}{N} \tag{11}$$

where Si represents the number of landslide pixels within the subclass; S refers to the pixel in the subclass; Ni is the number of landslide pixels in the entire area; N is the total number of pixels in the whole area.

Validation of susceptibility maps

Landslide susceptibility map validation is useful for identifying modeling constraints. Validation is performed by comparing the accuracy of both models and the selection of parameter variables. This study used the Area Under Curve of Receiver Operating Characteristics (AUC ROC) to determine model accuracy. The success rate curve was analyzed using 70% of the training data to assess the suitability of the existing landslide area classification. Meanwhile, the prediction rate curve assesses how well the model and conditioning factors identify landslides using the remaining landslide data in the future (Pradhan and Buchroithner 2010; Zhang et al. 2020; Dam et al. 2022; Aldiansyah and Wardani 2024a). Quantitatively, the model accuracy range is expressed as 0.9–1.0 = excellent, 0.8–0.9 = good, 0.7–0.8 = acceptable, 0.6–0.7 = poor, and 0.5–0.6 = failed (Yilmaz 2009).

Result

Application of Weight of Evidence model

The Weight of Evidence value for each conditioning factor is calculated based on Equation (8), and its relationship to landslide events is shown in Table 2. The greater the positive value (>0), the greater the potential for landslides, and vice versa. WoE analysis of the relationship between landslide events and slope shows that the >45° class has the highest value of 2.128. Other slope classes have a lower probability of experiencing landslides. The concave and convex curvature classes each have high WoE values (0.598 and 0.572, respectively) indicating a high possibility of landslides. Meanwhile, the flat curvature class shows a negative value (WoE = –0.522), signifying a low possibility of landslides. The aspect factor class that has the potential for landslides is almost shown by all classes even though with low abundance, except for the Flat, North East, East and South East classes, which have negative values. The most abundant lithology factor class is TQpm (WoE=0.924), which indicates that there is a high possibility of landslides in this formation. However, other classes such as Qtl and Tmtv have almost unaffected opportunities. The distance from fault factor class shows that classes 1000–2000 and 2000–3000 show high WoE values (1.345 and 1.163, respectively). Generally, the frequency of landslides will increase as the distance from road gets smaller. However, in this study, the possibility of landslides is high in the class with the furthest distance. This also occurs in the distance from river class. This is because continuous riverbank erosion by the Lindu River contributes significantly to landslide occurrence. Based on land use, the results of the study indicate that forest classes (primary and secondary dryland forest) each have a high probability of landslides (0.202 and 0.183). In NDVI, the factor class 0.09–0.40 shows the highest value (WoE=2.029), suggesting a higher probability of landslides. This range indicates open land, settlement areas and bushes. The other classes show WoE values <1 (except for classes –0.13–0.09 and 0.68–0.74, which are negative). The range of landslide occurrences at elevations of 763–926 m indicates a high landslide potential (WoE=2.7) in this area. Meanwhile, the height ranges 1,104–1,295, 125–1,503 and 2,009–2,373 m have low WoE values (0.139, 0.234 and 0.067, respectively), representing a lower probability of landslides. Generally, the frequency of landslides will be in line with increasing height. Based on precipitation, the ranges of 158–161, and 161–164 mm have higher WoE values compared to other classes with negative values. In the TWI factor, the probability of landslides is in the ranges of –8.81 to –7.22 and –7.22 to –5.62, although with low abundance. This is because excessive moisture accumulation on steep slopes can reduce slope stability. In the SPI factor, the probability of landslides tends to fluctuate as the SPI value increases. This is influenced by stronger erosion and soil erosion due to intense water flow. In the Profile Curvature class, the linear class has a low probability of experiencing landslides (–0.666), whereas the other classes have the opposite probability. The same thing is also shown by the plan curvature factor.

Application of Informative Value model

The relationship between landslide events and each factor is determined based on Equation (11) which will produce information values as shown in Table 2. The more negative the IV value, the smaller the possibility of landslides, and vice versa. The slope shows that >25° is very prone to landslides, with

Table 2. Data on landslide pixels and the outcomes derived from WoE and IV

Conditioning factors	Classes	Class pixels	Class pixels (%)	Landslide pixels	Landslide pixels (%)	WoE	IV
Slope	0–8	203,162	29.84	7	1.17	-3.236	-1.405
	8–15	173,907	25.54	76	12.75	-0.695	-0.302
	15–25	173,990	25.56	113	18.96	-0.299	-0.130
	25–45	102,650	15.08	202	33.89	0.811	0.352
	>45	27,099	3.98	198	33.22	2.128	0.921
Curvature	Concave	114,464	16.81	182	30.54	0.598	0.259
	Flat	450,271	66.14	234	39.26	-0.522	-0.226
	Convex	116,073	17.05	180	30.20	0.572	0.248
Aspect	Flat	37,846	5.56	0	0.00	-4.000	0
	North	43,897	6.45	45	7.55	0.158	0.069
	North East	71,070	10.44	45	7.55	-0.324	-0.141
	East	65,347	9.60	42	7.05	-0.309	-0.134
	South East	71,600	10.52	59	9.90	-0.061	-0.026
	South	77,928	11.45	77	12.92	0.121	0.053
	South West	96,775	14.21	108	18.12	0.243	0.105
	West	87,868	12.91	79	13.26	0.027	0.012
	North West	87,350	12.83	91	15.27	0.174	0.076
	North	41,127	6.04	50	8.39	0.329	0.143
Lithology	Qtl	37,124	5.45	0	0.00	0.001	0
	Tmtv	5,830	0.86	0	0.00	0.001	0
	Ql	148,483	21.81	83	13.93	-0.449	-0.195
	Kls	377,255	55.41	266	44.63	-0.217	-0.094
	TQpm	112,116	16.47	247	41.44	0.924	0.401
Distance from fault	0–1000	61,428	9.02	82	13.76	0.422	0.183
	1000–2000	59,674	8.77	200	33.56	1.345	0.583
	2000–3000	60,097	8.83	168	28.19	1.163	0.504
	3000–4000	56,290	8.27	61	10.23	0.214	0.093
	>4000	443,319	65.12	85	14.26	-1.519	-0.660
Distance from road	0–200	20,206	2.97	9	1.51	-0.676	-0.293
	200–400	19,657	2.89	17	2.85	-0.012	-0.005
	400–600	19,022	2.79	12	2.01	-0.328	-0.142
	600–800	18,519	2.72	13	2.18	-0.221	-0.096
	>800	603,404	88.63	545	91.44	0.031	0.014
Distance from river	0–100	24,242	3.56	15	2.52	-0.347	-0.151
	100–200	23,588	3.46	13	2.18	-0.463	-0.201
	200–300	22,866	3.36	10	1.68	-0.694	-0.301
	300–400	22,381	3.29	19	3.19	-0.031	-0.013
	>400	587,731	86.33	539	90.44	0.047	0.020
Land cover	Primary Dryland Forest	508,906	74.75	545	91.44	0.202	0.088
	Secondary Dryland Forest	34,252	5.03	36	6.04	0.183	0.079
	Bushes	11,690	1.72	0	0.00	0.001	0
	Settlement	160	0.02	0	0.00	0.001	0
	Open Land	113	0.02	0	0.00	0.001	0
	Water Body	38,659	5.68	0	0.00	0.001	0
	Dryland Agriculture	59,192	8.69	0	0.00	0.001	0
	Mix Dryland Agriculture	16,687	2.45	13	2.18	-0.117	-0.051
	Paddy Field	11,149	1.64	2	0.34	-1.586	-0.688

continuation on the next page

NDVI	-0.40 – -0.25	13,813	2.03	0	0.00	0.001	0
	-0.25 – -0.13	13,348	1.96	0	0.00	0.001	0
	-0.13–0.09	10,829	1.59	3	0.50	-1.151	-0.500
	0.09–0.40	2,265	0.33	15	2.52	2.029	0.879
	0.40–0.59	27,482	4.04	33	5.54	0.316	0.137
	0.59–0.68	90,723	13.33	99	16.61	0.221	0.096
	0.68–0.74	215,701	31.68	161	27.01	-0.160	-0.069
	0.74–0.87	306,647	45.04	285	47.82	0.060	0.026
Elevation	763–926	2,487	0.37	32	5.37	2.700	1.167
	926–1104	219,161	32.19	133	22.32	-0.367	-0.159
	1104–1295	133,219	19.57	134	22.48	0.139	0.060
	1295–1503	139,226	20.45	154	25.84	0.234	0.102
	1503–1735	121,363	17.83	99	16.61	-0.071	-0.031
	1735–2009	52,527	7.72	32	5.37	-0.363	-0.157
	2009–2373	12,825	1.88	12	2.01	0.067	0.029
Precipitation	152–158	177,623	26.09	109	18.29	-0.356	-0.154
	158–161	138,624	20.36	163	27.35	0.295	0.128
	161–164	110,167	16.18	129	21.64	0.291	0.126
	164–167	100,968	14.83	68	11.41	-0.262	-0.114
	167–170	74,594	10.96	76	12.75	0.152	0.066
	170–174	60,240	8.85	45	7.55	-0.159	-0.069
	174–179	18,592	2.73	6	1.01	-0.998	-0.433
TWI	-15.93 – -8.81	49,330	7.25	42	7.05	-0.028	-0.012
	-8.81 – -7.22	190,170	27.93	200	33.56	0.184	0.080
	-7.22 – -5.62	222,407	32.67	233	39.09	0.180	0.078
	-5.62 – -3.50	116,867	17.17	85	14.26	-0.185	-0.080
	-3.50–0.53	59,791	8.78	34	5.70	-0.432	-0.187
	0.53–5.09	40,476	5.95	2	0.34	-2.875	-1.248
	5.09–10.62	1,767	0.26	0	0.00	0.001	0
SPI	11.40–15.00	72,652	10.67	8	1.34	-2.074	-0.900
	15.00–16.11	212,462	31.21	141	23.66	-0.277	-0.120
	16.11–17.14	175,539	25.78	221	37.08	0.364	0.158
	17.14–18.32	134,715	19.79	131	21.98	0.105	0.046
	18.32–19.91	56,825	8.35	66	11.07	0.283	0.123
	19.91–22.26	22,151	3.25	22	3.69	0.126	0.055
	22.26–29.11	6,464	0.95	7	1.17	0.213	0.092
Profile Curvature	Concave	87,921	12.91	148	24.83	0.655	0.284
	Linear	273,401	40.16	123	20.64	-0.666	-0.289
	Convex	319,486	46.93	325	54.53	0.150	0.065
Plan Curvature	Convergence	205,370	30.17	234	39.26	0.264	0.114
	Linear	160,467	23.57	49	8.22	-1.054	-0.457
	Divergence	314,971	46.26	313	52.52	0.127	0.055

an IV value reaching 0.921. On the other hand, the flatter the slope, the lower the chance of landslides. In this study, landslide occurrences also increased as the slope angle increased. Regarding curvature, the flat class represents the lowest IV value (–0.226), where this value describes a low landslide possibility, while the Concave and Convex classes describe conditions that are inversely proportional to the flat class (0.256 and 0.248, respectively). The conditioning factor class aspect on the flat surface has no landslide abundance (IV=0), while all classes (except North East, East, and South East) show abundance with the highest abundance in the North and South West classes (–0.143 and 0.105), respectively, which indicate a fairly high probability of landslides. Lithological factors are also an important determinant in this research. The most abundant lithology factor class is in the Napu/TQpm formation class (IV=0.401), which indicates a high

probability of landslides. Distance from fault shows that the class between 1000 and 2000 m has the highest IV value (0.583), which indicates a higher possibility of landslides. Distance from road also shows that only classes >800 m have a landslide abundance (0.014) that indicates a possibility of landslides. The same thing is also shown by the distance from river factor, where only the farthest class shows the possibility of landslides (IV class >400 = 0.020). In terms of land use, rice fields and agriculture are considered to reduce the possibility of landslides, whereas forest areas have a high impact on the chances of landslides. NDVI class 0.09–0.68 has a high probability of landslides (average IV=0.370), whereas other classes representing negative IV values or low possibility. The elevation factor shows that class 763–926 m (IV=1.167) has a higher probability of landslides compared to other classes. Generally, landslides usually occur in relatively higher areas. However, in this study, landslides occurred at lower elevations. The relationship between precipitation and landslide occurrences shows that lower rainfall classes (158–161, 161–164, and 167–170 mm) show positive IV values or are likely to experience landslides. TWI classes –8.81 to –7.22 and –7.22 to –5.62 also have positive IV values (0.080 and 0.078, respectively). The SPI class of 16.11–29.11 has a high probability of experiencing landslides with positive IV, whereas other classes have low probabilities. In the Profile Curvature class, the linear class has a low probability of experiencing landslides with negative IV, whereas other classes have the opposite probability. The same is also shown by the plan curvature factor.

Landslide susceptibility map

The final value calculated for each pixel indicates its level of susceptibility to landslides. Higher LSM pixel values indicate higher susceptibility, whereas lower pixel values indicate lower susceptibility. The resulting LSM values have differences in the range of the WoE and IV models, namely ranging - 103–84 (Fig. 4a) and –6.31–3.93 (Fig. 4b), respectively. These values are then classified into very low, low, medium, high and very high susceptibility classes in the WoE and IV models. The classification in both models was carried out using the Jenks natural break method as visualized in Table 3.

Validation of landslide susceptibility maps

The models in this study were validated using the area under the curve (AUC) to test accuracy. The AUC curve is created by plotting the true positive rate (X-axis) against the false positive rate (Y-axis).

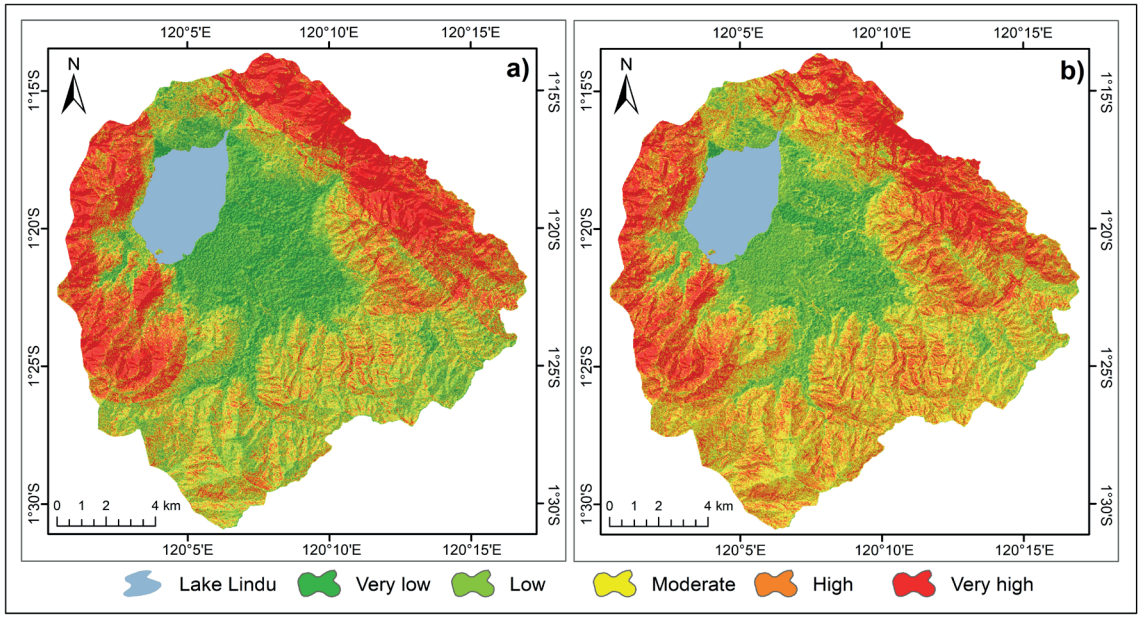

Fig. 4. Landslide susceptibility map based: a) weight of evidence (FR), and b) information values (IV) models

Table 3. Landslide susceptibility classes and summary of WoE and IV models

Landslide susceptibility class	WoE Model			IV Model		
	Range	Area (km²)	Area (%)	Range	Area (km²)	Area (%)
Very Low	-103 – -46	57.12	9.32	-6.31 – -3.43	72.12	11.76
Low	-46 – -22	118.40	19.31	-3.43 – -1.91	98.83	16.12
Moderate	-22 – -1	207.51	33.85	-1.91 – -0.59	161.33	26.31
High	-1–20	153.41	25.02	-0.59–0.56	184.74	30.13
Very High	20-84	76.69	12.51	0.56–3.93	96.10	15.67

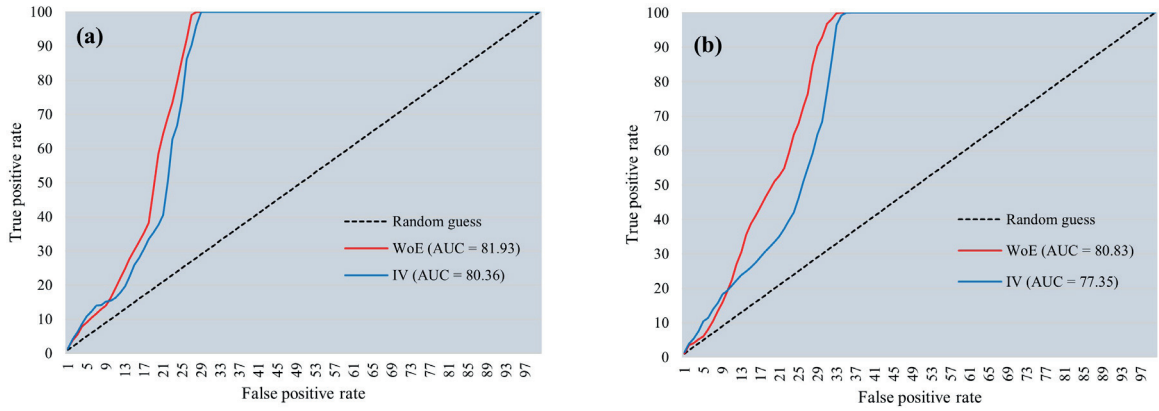

Fig. 5. The AUC of WoE and IV models: a) success rate curve, and b) prediction rate curve

The results show that the success rate curve values for both models are 81.93% and 80.36%, and the prediction rate curve values are 80.83% and 77.35% for the WoE and IV models, respectively. Success and prediction rate values between 0.8–0.9 indicate very good accuracy, while values between 0.7–0.8 indicate good accuracy (Fig. 5).

Discussion

This study divided homogeneous zones of the landslide susceptibility map based on varying levels of susceptibility. A total of 15 conditioning factors and a weighted landslide inventory were integrated to create both models. The WoE model is well known and reliable for mapping landslide likelihood, especially when integrated with slope instability (Bonham-Carter et al. 1989). This model excels compared to other models in terms of accuracy and ease of use (Dahal et al. 2012). Meanwhile, IV is commonly used for predicting landslide factor classes (Sarkar et al. 2008).

The training data for both models showed satisfactory agreement. However, minor differences remained between the models. The WoE model showed an AUC ROC value of 0.808, with a success rate of 81%. This study demonstrates the importance of selecting landslide-causing factors, which impact the accuracy of landslide susceptibility studies. Topography, environment, hydrology, geology and anthropogenic factors are commonly used and can be considered for landslide susceptibility modeling. This study uses two approaches to understand the conditioning factors and observed differences between data collected from the two models. The Napu formation (TQpm), which consists of sandstone, conglomerate and siltstone with intercalations of clay and peat, exhibits a high frequency of landslides. An increase in the density of geological boundaries indicates a close relationship with landslide events due to intensive weathering, transitions between different lithologies, and high tectonic activity. This finding is consistent in all reports with similar lithology (Kusumayudha and Ciptahening 2016). A continuous increase is indicated by an association with slope angles greater than 45°. The region consists of smaller areas (<4%) with steep slopes (>45°). This finding indicates that

Citation: Bulletin of Geography. Physical Geography Series 2026, 30, http://doi.org/10.12775/bgeo-2026-0005

the risk of landslides constantly increases with increasing slope gradient and then decreases, which aligns with findings from previous studies (Jaafari et al. 2014). This incident is caused by the increasing effects of gravity and shear stress (Wubalem 2020). The proportion of steep slope area and landslide area shows a correlation between steep slopes and landslide susceptibility. The northern slope has the highest concentration of landslides. Several landslide points were found relatively far from the road network and main river flows. This is thought to be related to the steep topography in the upstream area and the presence of weathering zones of volcanic rocks of the Napu Formation that have not been touched by slope stabilization activities. These findings are consistent with those found in several studies in mountainous areas (Ahmad et al. 2024; Bhandari et al. 2024; Dai et al. 2025; Tirsyayu et al. 2025). Model values indicate that landslides are concentrated near faults. Structural planes within fault zones cause rock fragmentation and weathering, forming significant deep weathering zones (Aldiansyah and Wardani 2024a). This is exacerbated by the erosive effects of rainfall on steep terrain, which further reduces soil shear forces and friction between the soil and bedrock (Aldiansyah and Wardani 2024a; 2024b). The results indicate that landslide susceptibility occurs in forested areas. This case was also reported in a study with similar morphology in Sulawesi (Tirsyayu et al. 2025). Identification using NDVI highlights the probability of landslides in open lands, settlements and bushes. According to Batar and Watanabe (2021), landslides generally occur in non-forest areas, considering that non-forest areas are susceptible to degradation. Although the cases are not directly proportional, similar results were also found in other studies (Mohammady et al. 2012; Ozdemir and Altural 2013; Teerarungsigul et al. 2016). The study area comprises 79% forest area and 21% non-forest area. The forest area is located on highlands and steep slopes. The results showed high landslide susceptibility in forest areas that have undergone significant landscape changes due to seismic activity, rainfall, tree root systems, tree weight and wind power (Greenway 1987; Beguería 2006). Therefore, high landslide susceptibility predominantly occurs at altitudes of 700–1500 m a.s.l. Most landslides can be attributed both to the lack of vegetation and to rainfall in the clay, marl and tuff framework areas in the upper catchment area and along the Lindu River, which flows south-westwards from the lake (Aldiansyah and Wardani 2024b). Both of these attributed factors are generally overlooked in landslide susceptibility mapping (Rawat et al. 2015). However, aspect actually influences the weathering and breakdown of rocks by sunlight. Landslide susceptibility is represented across nearly all slope aspect classes, although with relatively low abundance. However, the Flat, North East, East, and South East classes show negative values, indicating a lower contribution to landslide occurrence. The remaining aspect classes therefore pose potential risks to agricultural/plantation land and built-up areas. Potential slope aspects are also related to water flow direction, valley transitions, catchment areas, humidity and low sunlight, particularly in the Tomado and Puroo areas. Nevertheless, landslide mechanisms in Sulawesi are quite complex and are also influenced by geological conditions (Rohit et al. 2021) and other external factors (Patuti et al. 2017; Aldiansyah and Wardani 2024b). In addition to rainfall's role as a mineral lubricant that increases the likelihood of landslides, rainfall can also saturate the soil and increase groundwater levels. Therefore, human activities, material damage and casualties are at high risk from rainfall-induced landslides. Detailed geological information, high-resolution datasets and external spatial factors such as rainfall intensity/duration and earthquakes should be integrated into future landslide susceptibility mapping and assessments. Furthermore, we did not evaluate the role of temperature and groundwater in this landslide study, despite their known potential significant influence. These results are quite satisfactory for a local-scale study.

The models produced in this study were evaluated by the AUC. AUC measures map accuracy by comparing the success rate and prediction curves (Yesilnacar and Topal 2005). The success rate curve shows how well the model fits the identified landslides, while the prediction rate curve reflects the model's future prediction ability (Pradhan et al. 2010). A higher AUC value indicates greater accuracy, with values between 0.5 and 1.0 recommended for model evaluation (Yesilnacar and Topal 2005). AUC accuracy is classified as: excellent (0.9–1.0), very good (0.8–0.9), good (0.7–0.8), average (0.6–0.7) and fair (0.5–0.6) (Yesilnacar and Topal 2005). AUC values near 1.0 indicate ideal performance, whereas values ≤0.5 suggest poor performance (Fawcett 2006). All three landslide susceptibility maps have high accuracy, at >75%. The WoE model

is superior to model IV. This is indicated by the satisfactory level of agreement between the training data and validation data. The majority of pixels are classified correctly and have high sensitivity in distinguishing landslide occurrences. Pamela et al. (2018) used a single model of WoE and LR to compare landslide susceptibility mapping in the Takengon area, Aceh. According to statistics, the WoE model showed the highest AUC value of 0.830. In addition, the WoE model also showed the highest AUC value in East Ungaran, at 0.798 (Maulana et al. 2024). According to Paudyal et al. (2024), the WoE model has a higher accuracy than the FR and AHP models, at 89.9% for the entire data set. A study in Cianjur Regency, Indonesia showed that the IV model had the highest accuracy compared to WoE and FR, with success rates of 0.930, 0.926 and 0.920, respectively (Arifianti et al. 2020). Previous research conducted in the Cisangkuy Sub-Watershed showed that the IV model had good accuracy compared to WoE, SE and FR (Sukristiyanti et al. 2024). Fewer studies have compared these models in Indonesia. In the previous study, the WoE model was not always reliable. Therefore, there was no clear difference in prediction ratios between the models compared. However, the WoE model showed a tendency for better success and prediction ratios in Lindu District, Indonesia. This may be due to the area being less heterogeneous in vegetation, geological characteristics and morphology, making generalization easier, and to the numerous landslides identified at this scale. In some cases, relatively smaller study areas still have poorer accuracy (Nicu 2018; Panahi et al. 2022), and this is further exacerbated when fewer landslides are identified (Ilia and Tsangaratos 2016; Vakhshoori and Zare 2016). Although results are better in many cases, particularly at the basin scale (Conoscenti et al. 2016; Chen et al. 2018; Jia et al. 2023), causal factors also influence the results of these studies, in addition to the statistical methods and GIS software used.

Conclusion

This study demonstrates the reliability and effectiveness of GIS and bivariate statistical models in mapping landslide susceptibility zones in Lindu Regency, Indonesia. Key factors influencing landslides in Lindu District include elevation, slope, aspect, curvature, plan and profile curvature, SPI, TWI, road, river, fault, land use, NDVI, lithology and precipitation. Landslide inventories were sourced from Google Earth imagery, identifying and mapping 391 landslide locations. Landslide susceptibility models were categorized into five classes: very low, low, medium, high and very high. The AUC curve shows that the WoE model outperforms the IV model, with success rates of 81.93% and 80.36% and prediction rates of 80.83% and 77.35%, respectively. The results of this study can inform practical landslide mitigation strategies in Lindu District. For instance, high and very high susceptibility zones can be prioritized for early-warning system installations, slope stabilization projects and targeted reforestation efforts. The findings also support land-use planning by identifying areas unsuitable for infrastructure development due to high landslide risk. In terms of future perspective, the susceptibility maps produced in this study can serve as a vital tool for local governments in disaster risk reduction planning, guiding infrastructure development, and allocating resources more efficiently. Further research may integrate dynamic factors such as rainfall thresholds, real-time monitoring data, and machine learning models to enhance predictive accuracy and applicability in other landslide-prone regions of Indonesia.

Acknowledgements

The researchers would like to thank the staff and colleagues at the University of Indonesia, Halu Oleo University, and Lore Lindu National Park, Central Sulawesi, and fellow Institutions for their support and assistance. The researchers appreciate their valuable contributions to this research.

Disclosure statement

The authors declare that they have no conflict of interest.

Author contributions

Study design: SA, IM; data collection: SA; spatial analysis: SA, IM; statistical analysis: IM; result interpretation: IM, SA; manuscript preparation: SA, IM; literature review: SA.

References

ADDIS A, 2024, Landslide susceptibility mapping using GIS and bivariate statistical models in Chemoga Watershed, Ethiopia. *Advances in Civil Engineering* 2024(1): 6616269. DOI: https://doi.org/10.1155/2024/6616269.

AHMAD H, ALAM M, YINGHUA Z, NAJEH T, GAMIL Y, and HAMEED S, 2024, Landslide risk assessment integrating susceptibility, hazard, and vulnerability analysis in Northern Pakistan. *Discover Applied Sciences* 6(1): 7. DOI: https://doi.org/10.1007/s42452-024-05646-2.

ALDIANSYAH S and WARDANI F, 2024a, Assessment of resampling methods on performance of landslide susceptibility predictions using machine learning in Kendari City, Indonesia. *Water Practice and Technology* 19(1): 52-81. DOI: https://doi.org/10.2166/wpt.2024.002.

ALDIANSYAH S and WARDANI F, 2024b, Spatiotemporal dynamic of soil erosion in the Roraya River Basin based on RUSLE model and Google Earth Engine. *Journal of Hydroinformatics* 26(6): 1273-1294. DOI: https://doi.org/10.2166/hydro.2024.219.

ALDIANSYAH S, NINGSIH DSW, and SAPUTRA RA, 2023, Evaluation of Regional Spatial Development on Landslide and Flood Prone with Actual Site Conditions in Kendari City. *Jurnal Wilayah dan Lingkungan* 11(1): 92-107. DOI: http://dx.doi.org/10.14710/jwl.11.1.92-107.

ARIFIANTI Y, PAMELA P, AGUSTIN F and MUSLIM D, 2020, Comparative Study among Bivariate Statistical Models in Landslide Susceptibility Map. *Indonesian Journal on Geoscience* 7(1): 51–63. DOI: https://doi.org/10.17014/ijog.7.1.51-63.

AYALEW L and YAMAGISHI H, 2005, The application of GIS-based logistic regression for landslide susceptibility mapping in the Kakuda-Yahiko Mountains, Central Japan. *Geomorphology* 65(1-2): 15-31. DOI: https://doi.org/10.1016/j.geomorph.2004.06.010.

AYALEW L, YAMAGISHI H and UGAWA N, 2004, Landslide susceptibility mapping using GIS-based weighted linear combination, the case in Tsugawa area of Agano River, Niigata Prefecture, Japan. *Landslides* 1: 73-81. DOI: https://doi.org/10.1007/s10346-003-0006-9.

BAGENDA AF, UTOMO LP and RUSYDI M, 2020, Pemanfaatan GIS dalam Pemetaan Zonasi Kawasan Bahaya Banjir di Kabupaten Sigi. *Katalogis* 8(3): 260-269.

BATAR AK and WATANABE T, 2021, Landslide Susceptibility Mapping and Assessment Using Geospatial Platforms and Weights of Evidence (WoE) Method in the Indian Himalayan Region: Recent Developments, Gaps and Future Directions. *ISPRS International Journal of Geo-Information* 10(3): 114. DOI: https://doi.org/10.3390/ijgi10030114.

BEGUERÍA S, 2006, Changes in land cover and shallow landslide activity: a case study in the Spanish Pyrenees. *Geomorphology* 74(1-4): 196-206. DOI: https://doi.org/10.1016/j.geomorph.2005.07.018.

BHANDARI BP, DHAKAL S and TSOU CY, 2024, Assessing the Prediction Accuracy of Frequency Ratio, Weight of Evidence, Shannon Entropy and Information Value Methods for Landslide Susceptibility in the Siwalik Hills of Nepal. *Sustainability* 16(5): 2092. DOI: https://doi.org/10.3390/su16052092.

BONHAM-CARTER GF, AGTERBERG FP and WRIGHT DF, 1989, Integration of geological datasets for gold exploration in Nova Scotia. *Digital Geologic and Geographic Information Systems* 10: 15-23. DOI: https://doi.org/10.1029/SC010p0015.

BPS, 2024, Lindu District in Figure 2024. https://sigikab.bps.go.id/id/publication/2024/09/26/63beb709e17a0a6fa37fa043/kecamatan-lindu-dalam-angka-2024.html.

BRABB EE, 1984, Innovative Approaches to Landslide Hazard Mapping. *Proceedings of 4th International Symposium on Landslides* 1: 307-324.

CHEN W, XIE X, PENG J, SHAHABI H, HONG H, BUI DT, DUAN Z and ZHU AX, 2018, GIS-based landslide susceptibility evaluation using a novel hybrid integration approach of bivariate statistical based random forest method. *Catena* 164: 135-149. DOI: https://doi.org/10.1016/j.catena.2018.01.012.

CONOSCENTI C, ROTIGLIANO E, CAMA M, CARABALLO-ARIAS NA, LOMBARDO L and AGNESI V, 2016, Exploring the effect of absence selection on landslide susceptibility models: a case study in Sicily, Italy. *Geomorphology*, 261: 222-235. DOI: https://doi.org/10.1016/j.geomorph.2016.03.006.

DAHAL RK, HASEGAWA S, BHANDARY NP, POUDEL PP, NONOMURA A and YATABE R, 2012. A replication of landslide hazard mapping at catchment scale. *Geomatics, Natural Hazards and Risk* 3(2): 161-192. DOI: https://doi.org/10.1080/19475705.2011.629007.

DAI X, CHEN J, ZHANG T and XUE C, 2025, Integrated Landslide Risk Assessment via a Landslide Susceptibility Model Based on Intelligent Optimization Algorithms. *Remote Sensing* 17(3): 545. DOI: https://doi.org/10.3390/rs17030545.

DAM ND, AMIRI M, AL-ANSARI N, PRAKASH I, LE HV, NGUYEN HBT and PHAM BT, 2022, Evaluation of Shannon entropy and weights of evidence models in landslide susceptibility mapping for the pithoragarh district of Uttarakhand state, India. *Advances in Civil Engineering* 2022(1): 6645007. DOI: https://doi.org/10.1155/2022/6645007.

DATA INFORMASI BENCANA INDONESIA (DIBI), 2024, Statistik Bencana, Korban, dan Kerusakan Menurut Wilayah. Available at: https://dibi.bnpb.go.id/statistik_menurut_wilayah.

DING Q, CHEN W and HONG H, 2017, Application of frequency ratio, weights of evidence and evidential belief function models in landslide susceptibility mapping. *Geocarto international* 32(6): 619-639. DOI: https://doi.org/10.1080/10106049.2016.1165294.

DU GL, ZHANG YS, IQBAL J, YANG ZH and YAO X, 2017, Landslide susceptibility mapping using an integrated model of information value method and logistic regression in the Bailongjiang watershed, Gansu Province, China. *Journal of Mountain Science* 14: 249-268. DOI: https://doi.org/10.1007/s11629-016-4126-9.

ES-SMAIRI A, ELMOUTCHOU B, MIR RA, TOUHAMI AEO and NAMOUS M, 2023, Delineation of landslide susceptible zones using Frequency Ratio (FR) and Shannon Entropy (SE) models in northern Rif, Morocco. *Geosystems and Geoenvironment* 2(4): 100195. DOI: https://doi.org/10.1016/j.geogeo.2023.100195.

FAWCETT T, 2006, An introduction to ROC analysis. *Pattern recognition letters* 27(8): 861-874. DOI: https://doi.org/10.1016/j.patrec.2005.10.010.

GREENWAY DR, 1987, Vegetation and slope stability. In: Anderson MG, Richards KS (eds), *Slope stability*. Wiley, Chichester.

GÓMEZ D, GARCÍA EF and ARISTIZÁBAL E, 2023, Spatial and temporal landslide distributions using global and open landslide databases. *Natural Hazards* 117(1): 25-55. DOI: https://doi.org/10.1007/s11069-023-05848-8.

HADMOKO DS, WIBOWO SB, SIANIPAR DSJ, DARYONO D, FATHONI MN, PRATIWI RS, HARYONO E and LAVIGNE F, 2024, Co-seismic deformation and related hazards associated with the 2022 Mw 5.6 Cianjur earthquake in West Java, Indonesia: insights from combined seismological analysis, DInSAR and geomorphological investigations. *Geoenvironmental Disasters* 11(1): 15. DOI: https://doi.org/10.1186/s40677-024-00277-6.

HE S, PAN P, DAI L, WANG H and LIU J, 2012, Application of kernel-based Fisher discriminant analysis to map landslide susceptibility in the Qinggan River delta, Three Gorges, China. *Geomorphology* 171: 30-41. DOI: https://doi.org/10.1016/j.geomorph.2012.04.024.

HUANG S and CHEN L, 2024, Landslide susceptibility mapping using an integration of different statistical models for the 2015 Nepal earthquake in Tibet. *Geomatics, Natural Hazards and Risk* 15(1): 2396908. DOI: https://doi.org/10.1080/19475705.2024.2396908.

HUNGR O, LEROUEIL S and PICARELLI L, 2014, The Varnes classification of landslide types, an update. *Landslides* 11(2): 167-194. DOI: https://doi.org/10.1007/s10346-013-0436-y.

HUSSAIN Y, CARDENAS-SOTO M, MARTINO S, MOREIRA C, BORGES W, HAMZA O, PRADO R, UAGODA R, RODRÍGUEZ-REBOLLEDO J, SILVA RC and MARTINEZ-CARVAJAL H, 2019, Multiple Geophysical Techniques for Investigation and Monitoring of Sobradinho Landslide, Brazil. *Sustainability* 11(23): 6672. DOI: https://doi.org/10.3390/su11236672.

ILIA I and TSANGARATOS P, 2016, Applying weight of evidence method and sensitivity analysis to produce a landslide susceptibility map. *Landslides* 13: 379-397. DOI: https://doi.org/10.1007/s10346-015-0576-3.

JAAFARI A, NAJAFI A, POURGHASEMI HR, REZAEIAN J and SATTARIAN A, 2014, GIS-based frequency ratio and index of entropy models for landslide susceptibility assessment in the Caspian forest, northern Iran. *International Journal of Environmental Science and Technology* 11: 909-926. DOI: https://doi.org/10.1007/s13762-013-0464-0.

JALIL A, FATHANI TF, SATYARNO I and WILOPO W, 2021, Liquefaction in Palu: the cause of massive mudflows. *Geoenvironmental Disasters* 8(1): 21. DOI: https://doi.org/10.1186/s40677-021-00194-y.

JIA W, WEN T, LI D, GUO W, QUAN Z, WANG Y, HUANG D and HU M, 2023, Landslide Displacement Prediction of Shuping Landslide Combining PSO and

LSSVM Model. *Water* 15(4): 612. DOI: https://doi.org/10.3390/w15040612.

KHAN H, SHAFIQUE M, KHAN MA, BACHA M A, SHAH SU and CALLIGARIS C, 2019, Landslide susceptibility assessment using Frequency Ratio, a case study of northern Pakistan. *The Egyptian Journal of Remote Sensing and Space Science* 22(1): 11-24. DOI: https://doi.org/10.1016/j.ejrs.2018.03.004.

KUSUMAYUDHA SB and CIPTAHENING AN, 2016, Correlation between Tectonic Environment and Chracteristics of Mass Movement (Landslides): A Case Study from Java, Indonesia. *Journal of Geological resource and Engineering* 4(2): 51-62. http://eprints.upnyk.ac.id/id/eprint/9028.

LEE S and CHOI J, 2004, Landslide susceptibility mapping using GIS and the weight-of-evidence model. *International Journal of Geographical Information Science* 18(8): 789-814. DOI: https://doi.org/10.1080/13658810410001702003.

LEE S and PRADHAN, B, 2007, Landslide hazard mapping at Selangor, Malaysia using frequency ratio and logistic regression models. *Landslides*, 4(1): 33-41. DOI: https://doi.org/10.1007/s10346-006-0047-y.

MARTENS D, VANTHIENEN J, VERBEKE W and BAESENS B, 2011, Performance of classification models from a user perspective. *Decision Support Systems*, 51(4): 782-793. DOI: https://doi.org/10.1016/j.dss.2011.01.013.

MAULANA DS, INDRAWAN IGB and WARMADA IW, 2024, Landslide susceptibility mapping in East Ungaran, Indonesia: A comparative study using statistical methods. *Journal of Degraded and Mining Lands Management* 11(4): 6107–6120. DOI: https://doi.org/10.15243/jdmlm.2024.114.6107.

MEHRABI M and MOAYEDI H, 2021, Landslide susceptibility mapping using artificial neural network tuned by metaheuristic algorithms. *Environmental Earth Sciences* 80(24): 804. DOI: https://doi.org/10.1007/s12665-021-10098-7.

MOHAMMADY M, POURGHASEMI HR and PRADHAN B, 2012, Landslide susceptibility mapping at Golestan Province, Iran: a comparison between frequency ratio, Dempster–Shafer and weights-of-evidence models. *Journal of Asian Earth Sciences* 61: 221-236. DOI: https://doi.org/10.1016/j.jseaes.2012.10.005.

NGADISIH, SAMODRA G, BHANDARY NP and YATABE R, 2017, Landslide inventory: challenge for landslide hazard assessment in Indonesia. *GIS landslide* 135-159. DOI: https://doi.org/10.1007/s11069-023-05848-8.

NICU IC, 2017, Frequency ratio and GIS-based evaluation of landslide susceptibility applied to cultural heritage assessment. *Journal of Cultural Heritage* 28: 172-176. DOI: https://doi.org/10.1016/j.culher.2017.06.002.

OH HJ, LEE S and HONG SM, 2017, Landslide susceptibility assessment using frequency ratio technique with iterative random sampling. *Journal of Sensors* 2017(1): 3730913. DOI: https://doi.org/10.1155/2017/3730913.

PANCHAL S and SHRIVASTAVA AK, 2021, A comparative study of frequency ratio, Shannon's entropy and analytic hierarchy process (AHP) models for landslide susceptibility assessment. *ISPRS International Journal of Geo-Information* 10(9): 603. DOI: https://doi.org/10.3390/ijgi10090603.

PAUDYAL KR, MAHARJAN R, SHRESTHA B and MAHARJAN N, 2024, A Comparative of Frequency Ratio Method, Weight of Evidence and Analytical Hierarchy Process for Landslide Susceptibility Assessment in the Main Boundary Thrust (MBT) Region in Ranitar-Belarang Section of Udayapur District, Koshi Province, Nepal. *Earth Sciences Research Journal* 28(3): 325. DOI: https://doi.org/10.15446/esrj.v28n3.112740.

PHAM BT, BUI DT, DHOLAKIA MB, PRAKASH I, PHAM HV, MEHMOOD K and LE HQ, 2017, A novel ensemble classifier of rotation forest and Naïve Bayer for landslide susceptibility assessment at the Luc Yen district, Yen Bai Province (Viet Nam) using GIS. Geomatics, *Natural Hazards and Risk* 8(2): 649-671. DOI: https://doi.org/10.1080/19475705.2016.1255667.

OZDEMIR A and ALTURAL T, 2013, A comparative study of frequency ratio, weights of evidence and logistic regression methods for landslide susceptibility mapping: Sultan Mountains, SW Turkey. *Journal of Asian Earth Sciences* 64: 180-197. DOI: https://doi.org/10.1016/j.jseaes.2012.12.014.

PAMELA P, SADISUN IA, KARTIKO RD and ARIFIANTI Y, 2018, Metode Kombinasi Weight of Evidence (WoE) dan Logistic Regression (LR) untuk Pemetaan Kerentanan Gerakan Tanah di Takengon, Aceh. *Jurnal Lingkungan dan Bencana Geologi* 9(2): 77-86..

PANAHI M, RAHMATI O, REZAIE F, LEE S, MOHAMMADI F and CONOSCENTI C, 2022, Application of the group method of data handling (GMDH) approach for landslide susceptibility zonation using readily available spatial covariates. *Catena* 208: 105779. DOI: https://doi.org/10.1016/j.catena.2021.105779.

PATUTI IM, RIFA'I A and SURYOLELONO KB, 2017, Mechanism and characteristics of the landslides in Bone Bolango regency, Gorontalo province, Indone-

sia. *Geomate Journal* 12(29), 1-8. DOI: http://dx.doi.org/10.21660/2017.29.79901.

PRADHAN B, LEE S and BUCHROITHNER MF, 2010, Remote sensing and GIS-based landslide susceptibility analysis and its cross-validation in three test areas using a frequency ratio model. *Photogrammetrie-Fernerkundung-Geoinformation* 2020: 17-32. DOI: https://doi.org/10.1127/1432-8364/2010/0037.

RAWAT MS, UNIYAL DP, DOBHAL R, JOSHI V, RAWAT BS, BARTWAL A, SINGH D and ASWAL A, 2015, Study of landslide hazard zonation in Mandakini Valley, Rudraprayag district, Uttarakhand using remote sensing and GIS. *Current Science* 109(1): 158-170.

REGMI AD, DEVKOTA KC, YOSHIDA K, PRADHAN B, POURGHASEMI HR, KUMAMOTO T, dan AKGUN A, 2014, Application of frequency ratio, statistical index and weights-of-evidence models and their comparison in landslide susceptibility mapping in Central Nepal Himalaya. *Arabian Journal of Geosciences* 7: 725-742. DOI: https://doi.org/10.1007/s12517-012-0807-z.

ROHIT D, HAZARIKA H, MAEDA T, SUMARTINI WO, KOKUSHO T, MANAFI KHAJEH PASHA, S and NURDIN S, 2021, Forensic investigation of flowslides triggered by the 2018 Sulawesi earthquake. *Progress in Earth and Planetary Science* 8: 1-20. DOI: https://doi.org/10.1186/s40645-021-00452-5.

SARKAR S, KANUNGO DP, PATRA AK and KUMAR P, 2008, GIS based spatial data analysis for landslide susceptibility mapping. *Journal of Mountain Science* 5: 52-62. DOI: https://doi.org/10.1007/s11629-008-0052-9.

SHU H, GUO Z, QI S, SONG D and POURGHASEMI HR, MA J, 2021, Integrating landslide typology with weighted frequency ratio model for landslide susceptibility mapping: A case study from Lanzhou city of northwestern China. *Remote Sensing* 13(18): 3623. DOI: https://doi.org/10.3390/rs13183623.

SIVAKAMI C and RAJKUMAR DR, 2020, Landslide vulnerability zone by weights of evidence model using remote sensing and GIS, in kodaikanal taluk (Tamil nadu, India). *International Journal of Engineering Research* 9(2): 788-793. DOI: http://dx.doi.org/10.17577/IJERTV9IS020201.

SUBIYANTORO A, VAN WESTEN CJ, DEN BOUT BV, YUNIAWAN RA and MULYANA AR, 2022, November. Semi-automatic landslide detection using Google Earth engine, a case study in Poi Village, Central Sulawesi. *In 2022 IEEE International Conference on Aerospace Electronics and Remote Sensing Technology* (ICARES), 1-4.

SUKRISTIYANTI S, PAMELA, SAFITRI S, HADIYANTO AL, TOHARI A and SADISUN IA, 2024, The Performance of Bivariate Statistical Models in Landslide Susceptibility Mapping (Case Study: Cisangkuy Sub-Watershed, Bandung, Indonesia). *Rudarsko-geološko-Naftni Zbornik* 39(5): 19–39. DOI: https://doi.org/10.17794/rgn.2024.5.2.

TANG RX, KULATILAKE PH, YAN EC and CAI JS, 2020, Evaluating landslide susceptibility based on cluster analysis, probabilistic methods and artificial neural networks. *Bulletin of Engineering Geology and the Environment* 79: 2235-2254. DOI: https://doi.org/10.1007/s10064-019-01684-y.

TEERARUNGSIGUL S, TORIZIN J, FUCHS M, KÜHN F and CHONGLAKMANI C, 2016, An integrative approach for regional landslide susceptibility assessment using weight of evidence method: a case study of Yom River Basin, Phrae Province, Northern Thailand. *Landslides* 13: 1151-1165. DOI: https://doi.org/10.1007/s10346-015-0659-1.

TIRSYAYU T, SOMA AS and PAEMBONAN SA, 2025, Land use direction based on landslide susceptibility levels in the Rongkong Watershed, South Sulawesi, Indonesia. *Asian Journal of Forestry* 9(1): 53-66. DOI: https://doi.org/10.13057/asianjfor/r090106.

TURNER AK and SCHUSTER RL, 1996, Landslides: investigation and mitigation: Transportation research board special report 247. National Research Council, Washington, DC, 673. http://onlinepubs.trb.org/Onlinepubs/sr/sr247/sr247.pdf.

UMAR Z, PRADHAN B, AHMAD A, JEBUR MN and TEHRANY MS, 2014, Earthquake induced landslide susceptibility mapping using an integrated ensemble frequency ratio and logistic regression models in West Sumatera Province, Indonesia. *Catena* 118: 124-135. DOI: https://doi.org/10.1016/j.catena.2014.02.005.

VAN DEN EECKHAUT M, POESEN J, VERSTRAETEN G, VANACKER V, MOEYERSONS J, NYSSEN J and VAN BEEK LPH, 2005, The effectiveness of hillshade maps and expert knowledge in mapping old deep-seated landslides. *Geomorphology* 67(3-4): 351-363. DOI: https://doi.org/10.1016/j.geomorph.2004.11.001.

VAKHSHOORI V and ZARE M, 2016, Landslide susceptibility mapping by comparing weight of evidence, fuzzy logic and frequency ratio methods. *Geomatics, Natural Hazards and Risk* 7(5): 1731-1752. https://doi.org/10.1080/19475705.2016.1144655.

WANG LJ, GUO M, SAWADA K, LIN J and ZHANG J, 2016, A comparative study of landslide susceptibility maps using logistic regression, frequency ratio, decision tree, weights of evidence and artificial neural network. *Geosciences Journal* 20: 117-136. DOI: https://doi.org/10.1007/s12303-015-0026-1.

WUBALEM A, 2020, Modeling of Landslide susceptibility in a part of Abay Basin, northwestern Ethiopia. *Open Geosciences* 12(1): 1440-1467. DOI: https://doi.org/10.1515/geo-2020-0206.

XU C, DAI F, XU X and LEE YH, 2012, GIS-based support vector machine modeling of earthquake-triggered landslide susceptibility in the Jianjiang River watershed, China. *Geomorphology* 145: 70-80. DOI: https://doi.org/10.1016/j.geomorph.2011.12.040.

YANG ZH, LAN HX, GAO X, LI LP, MENG YS and WU YM, 2015, Urgent landslide susceptibility assessment in the 2013 Lushan earthquake-impacted area, Sichuan Province, China. *Natural Hazards* 75: 2467-2487. DOI: https://doi.org/10.1007/s11069-014-1441-8.

YESILNACAR E and TOPAL TAMER, 2005, Landslide susceptibility mapping: a comparison of logistic regression and neural networks methods in a medium scale study, Hendek region (Turkey). *Engineering Geology* 79(3-4): 251-266. DOI: https://doi.org/10.1016/j.enggeo.2005.02.002.

YILMAZ I, 2009, Landslide susceptibility mapping using frequency ratio, logistic regression, artificial neural networks and their comparison: a case study from Kat landslides (Tokat—Turkey). *Computers and Geosciences* 35(6): 1125-1138. DOI: https://doi.org/10.1016/j.cageo.2008.08.007.

YUSRAN Y, ERNIWATI E, KHUMAIDI A, PITOPANG R and JATI IRAP, 2023, Diversity of substrate type, ethnomycology, mineral composition, proximate and phytochemical compounds of the Schizopyllum commune Fr. in the area along Palu-Koro Fault, Central Sulawesi, Indonesia. *Saudi Journal of Biological Sciences* 30(4): 103593. DOI: https://doi.org/10.1016/j.sjbs.2023.103593.

ZHANG YX, LAN HX, LI LP, WU YM, CHEN JH and TIAN NM, 2020, Optimizing the frequency ratio method for landslide susceptibility assessment: A case study of the Caiyuan Basin in the southeast mountainous area of China. *Journal of Mountain Science* 17(2): 340-357. DOI: https://doi.org/10.1007/s11629-019-5702-6.

Received 7 January 2026
Accepted 11 July 2025